Original Article

MOLECULAR METABOLISM

Liver-specific *Prkn* knockout mice are more susceptible to diet-induced hepatic steatosis and insulin resistance

Lia R. Edmunds [1], Bingxian Xie [1], Amanda M. Mills [1], Brydie R. Huckestein [1], Ramya Undamatla [1], Anjana Murali [1], Martha M. Pangburn [1], James Martin [2,3], Ian Sipula [1], Brett A. Kaufman [2,3], Iain Scott [2,3], Michael J. Jurczak [1,3,*]

ABSTRACT

Objective: PARKIN is an E3 ubiquitin ligase that regulates mitochondrial quality control through a process called mitophagy. Recent human and rodent studies suggest that loss of hepatic mitophagy may occur during the pathogenesis of obesity-associated fatty liver and contribute to changes in mitochondrial metabolism associated with this disease. Whole-body *Prkn* knockout mice are paradoxically protected against diet-induced hepatic steatosis; however, liver-specific effects of *Prkn* deficiency cannot be discerned in this model due to pleotropic effects of germline *Prkn* deletion on energy balance and subsequent protection against diet-induced obesity. We therefore generated the first liver-specific *Prkn* knockout mouse strain (LKO) to directly address the role of hepatic *Prkn*.

Methods: Littermate control (WT) and LKO mice were fed regular chow (RC) or high-fat diet (HFD) and changes in body weight and composition were measured over time. Liver mitochondrial content was assessed using multiple, complementary techniques, and mitochondrial respiratory capacity was assessed using Oroboros O_2K platform. Liver fat was measured biochemically and assessed histologically, while global changes in hepatic gene expression were measured by RNA-seq. Whole-body and tissue-specific insulin resistance were assessed by hyperinsulinemic-euglycemic clamp with isotopic tracers.

Results: Liver-specific deletion of *Prkn* had no effect on body weight or adiposity during RC or HFD feeding; however, hepatic steatosis was increased by 45% in HFD-fed LKO compared with WT mice ($P < 0.05$). While there were no differences in mitochondrial content between genotypes on either diet, mitochondrial respiratory capacity and efficiency in the liver were significantly reduced in LKO mice. Gene enrichment analyses from liver RNA-seq results suggested significant changes in pathways related to lipid metabolism and fibrosis in HFD-fed *Prkn* knockout mice. Finally, whole-body insulin sensitivity was reduced by 35% in HFD-fed LKO mice ($P < 0.05$), which was primarily due to increased hepatic insulin resistance (60% of whole-body effect; $P = 0.11$).

Conclusions: These data demonstrate that PARKIN contributes to mitochondrial homeostasis in the liver and plays a protective role against the pathogenesis of hepatic steatosis and insulin resistance.

Keywords Parkin; Mitochondria; Mitophagy; Bioenergetics; Hepatic steatosis; Insulin resistance

1. INTRODUCTION

The number of overweight and obese individuals in the U.S. increased dramatically over the last two decades. With this increase, the prevalence of several obesity-associated metabolic diseases, such as type 2 diabetes and non-alcoholic fatty liver disease (NAFLD), similarly skyrocketed. Current estimates suggest that 10.5% of the U.S. population or 34.2 million Americans have diabetes [1], and 30% of the U.S. population has NAFLD [2]. There is a strong positive association between type 2 diabetes and NAFLD, and estimates suggest greater than 70% of patients with type 2 diabetes have NAFLD [3,4]. NAFLD encompasses a range of hepatocellular alterations, including simple steatosis and steatosis with inflammation (NASH), which can lead to fibrosis, cirrhosis and hepatocellular carcinoma. Insulin resistance is considered a key pathogenic feature of NAFLD, in which compensatory hyperinsulinemia may promote steatosis through lipogenesis or lipid oversupply to the liver may drive steatosis, in turn inducing insulin resistance [5]. In addition to insulin resistance, changes in mitochondrial metabolism are thought to contribute to the pathogenesis of NAFLD [6]; however, the relationship between insulin resistance, steatosis, and mitochondrial function in the liver remains incompletely understood.

Data from a growing number of human studies demonstrates changes in hepatic mitochondrial metabolism that occur during and potentially

[1]Division of Endocrinology and Metabolism, Department of Medicine, University of Pittsburgh, Pittsburgh, PA, USA [2]Division of Cardiology, Department of Medicine, University of Pittsburgh, Pittsburgh, PA, USA [3]Center for Metabolism and Mitochondrial Medicine, University of Pittsburgh, Pittsburgh, PA, USA

*Corresponding author. Department of Medicine, University of Pittsburgh, 200 Lothrop Street, BST W1060 Pittsburgh, PA 15213, USA. Fax: +412 648 3290. E-mail: jurczakm@pitt.edu (M.J. Jurczak).

Received May 12, 2020 • Revision received July 1, 2020 • Accepted July 7, 2020 • Available online 10 July 2020

https://doi.org/10.1016/j.molmet.2020.101051

Abbreviations

NAFLD	Non-alcoholic fatty liver disease
NASH	non-alcoholic steatohepatitis
HFD	high-fat diet
RCR	respiratory control ration
CCR	coupling control ratio
P_I/E	flux control ratio for complex I-mediated oxidative phosphorylation relative to maximal electron transport chain capacity
ETC	electron transport chain
OXPHOS	oxidative phosphorylation
NAS	NAFLD activity score
GIR	glucose infusion rate
EGP	endogenous or hepatic glucose production
STAR	Spliced Transcripts Alignment to a Reference
GO	gene ontology
KEGG	Kyoto Encyclopedia of Genes and Genomes
mtDNA	mitochondrial DNA
WT	wild-type
LKO	liver-specific *Prkn* knockout

contribute to the pathogenesis of type 2 diabetes and NAFLD. Hepatic mitochondrial structural defects and increased oxidative stress are positively associated with insulin resistance and steatosis in patients with NAFLD and NASH [7,8]. Hepatic adenosine triphosphate (ATP) turnover, a surrogate for mitochondrial function, is reduced in patients with type 2 diabetes or NASH [9,10]. More recently, Roden et al. assessed mitochondrial respiratory capacity using liver biopsies from lean healthy controls, obese patients with and without steatosis, and obese patients with NASH [11]. Mitochondrial respiratory capacity was increased in obese subjects with and without fatty liver compared with controls, although there was no change in mitochondrial mass, while mitochondrial respiratory capacity was reduced, despite increased mitochondrial mass, in patients with NASH compared with the lean and obese groups [11]. These observations suggest that energy excess that is common in obesity increases the metabolic load placed on hepatic mitochondria, inducing adaptations to buffer this load, which eventually fail.

Mitochondrial function and mass are maintained in part by balancing the production of new mitochondria through mitochondrial biogenesis and removal of damaged mitochondria by mitophagy. Mitophagy is a quality control pathway that regulates selective removal of damaged mitochondria from the cell, and multiple, independent studies demonstrate that impaired mitophagy results in abnormal mitochondrial function [12—16]. Recently, diet-induced obesity in mice has been reported to be associated with reduced rates of hepatic mitophagy, raising the intriguing possibility that defective hepatic mitophagy enhances obesity-associated liver metabolic disease and contributes to the pathogenesis of NAFLD [17]. While multiple forms of mitophagy exist, the PINK1-PARKIN-axis is the most well-described regulatory mechanism for selective, damage-induced mitophagy [18]. PARKIN is a ubiquitin E3 ligase that moves from the cytosol to the outer mitochondrial membrane in response to mitochondrial dysfunction, where it is phosphorylated and activated by PINK1 [19—22]. PARKIN then contributes to the generation of a phosphorylated ubiquitin signaling motif that marks the damaged mitochondria for degradation following recruitment of autophagy receptors [23—25].

Evidence of PARKIN's role in mitochondrial quality control comes from a number of *in vivo* studies in model systems, including *drosophila* and mice, which in general present with increased susceptibility to stress in various forms following deletion of *Prkn* [13,15,16,26—28]. Whole-body *Prkn* knockout mice are protected from nutritional stress in the liver and do not develop steatosis when fed a high-fat diet (HFD) [29,30], an apparently counterintuitive observation. However, these effects appear to be secondary to the protection of these mice from HFD-induced obesity, since obesity is strongly associated with the development of hepatic steatosis. Indeed, we recently reported that altered intestinal lipid absorption in the *Prkn* knockout mouse limits the liver's exposure to dietary stress, establishing that the primary and secondary effects of *Prkn* deletion on liver metabolism during HFD feeding cannot be defined in this model [31]. We therefore generated the first liver-specific *Prkn* knockout mouse strain (LKO) to determine the role of hepatic PARKIN with regard to mitochondrial function and lipid accrual during HFD feeding. In contrast to the currently held paradigm regarding PARKIN's role in liver during HFD-feeding, we find that LKO mice are more susceptible to diet-induced hepatic steatosis and insulin resistance, and that the pathogenesis of NAFLD in the absence of hepatic PARKIN is enhanced.

2. MATERIAL AND METHODS

2.1. Animal care and use

Mice were bred, housed and studied at the University of Pittsburgh according to guidelines established by the Institutional Care and Use Committee. All diets, interventions, and experimental procedures involving mice were reviewed and approved prior to studies. Liver-specific *Prkn* knockout mice were generated as described in the Results section. To control for sexual dimorphic effects on *Cre* expression, male mice hemizygous for *Cre* (*Cre*$^{+/-}$) and homozygous for the floxed *Prkn* allele (*Prkn*$^{fl/fl}$) were bred to females negative for *Cre* (*Cre*$^{-/-}$) and homozygous for the floxed *Prkn* allele. Littermate *Prkn*$^{fl/fl}$/*Cre*$^{+/-}$(LKO) and *Prkn*$^{fl/fl}$/*Cre*$^{-/-}$ (WT) were used for studies. Mice were housed at 22 ± 2 °C and provided free access to food and water, except where noted. For dietary studies, mice were fed a regular chow diet (RC; ProLab IsoPro RMH 3,000; kcal provided as approximately 26% protein, 14% fat, and 60% carbohydrate) beginning at six weeks of age. At 12 weeks old, mice were maintained on RC or provided a high-fat diet (HFD; Research Diets D12492; kcal provided as approximately 20% protein, 60% fat, and 20% protein) for 12 weeks. All diets were irradiated prior to use. Body weight was tracked weekly for nine weeks beginning at 12 weeks of age for both dietary studies and final body composition (fat and lean mass) was measured by EchoMRI. Mice were studied or euthanized for tissue collection at the end of the dietary studies after a six-hour morning fast (7 am—1 pm) for all studies, except where noted.

2.2. Protein isolation and western blotting

Protein immunoblotting was performed as previously described [30]. Briefly, frozen, pulverized liver was homogenized in radio-immunoprecipitation buffer (RIPA; 150 mM NaCl, 1.0% Triton X-100, 0.5% sodium deoxycholate, 0.1% sodium dodecyl sulfate, 50 mM Tris, pH 8.0) and centrifuged at 4 °C, 1,000× g to produce a post-nuclear supernatant. Protein concentration of the lysate was determined using BCA protein assay, and equal protein was loaded and resolved using Bolt Bis-Tris Plus gels prior to transfer to nitrocellulose membranes for incubation with antibodies as noted below. Immunoblots were developed with Licor Odyssey CLx using Licor IRDye goat secondary antibodies and analyzed using Licor Image Studio Software (Version 5.2). Primary antibodies were as follows: PARKIN (Santa Cruz sc-32282), OXPHOS antibody cocktail (Abcam ab110413), HSP60 (Cell Signaling

12165D), VDAC (Cell Signaling 4661S), SDHA (Cell Signaling 11998S), PHB1 (Cell Signaling 2426S), phospho-AKT^{SER473} (Cell Signaling 4060), AKT (Cell Signaling 2920), and GAPDH (Santa Cruz sc-25778 and sc-365062).

2.3. Biochemical analyses

Citrate synthase activity was determined as previously described [32]. Briefly, a mitochondrially enriched supernatant was prepared by homogenizing a 100-mg piece of liver in 1 ml of STE buffer (250 mM sucrose, 10 mM Tris—HCl, 1 mM EDTA) with a glass vessel and Teflon pestle, followed by centrifugation at 800× g for 10 min at 4 °C. Citrate synthase activity was then measured by mixing the mitochondrially enriched fraction with citrate synthase activity buffer (0.25% Triton X-100, 0.31 mM acetyl-CoA, 0.1 mM 5,5′-dithiobis(2-nitrobenzoic acid), 0.1 M triethanolamine, 1 mM EDTA, and 1 M Tris—HCl), followed by addition of 5 mM of oxaloacetate to initiate the reaction. The change in absorbance at 412 nm was recorded every 10 s over a 2-min period using a spectrophotometer set to 37 °C, and activity was calculated as the slope from the linear portion of the curve and normalized to the protein concentration determined by BCA protein assay. Plasma glucose levels were measured using an Analox GM9 Glucose Analyzer via the glucose oxidase method. Plasma insulin levels were measured using a Stellux Chemiluminescent Rodent Insulin ELISA (Alpco). Plasma and liver triglycerides were measured using Infinity Triglyceride Reagent (Thermo Fisher TR22421). Hepatic triglycerides were extracted using a methanol/chloroform-based method [30]. Plasma cholesterol levels were measured using Wako Diagnostics Total Cholesterol Kit (999-02601). Plasma liver enzymes were measured using Thermo Fisher Infinity Alanine Aminotransferase and Aspartate Aminotranferase activity kits (TR71121, TR70121). Plasma fatty acids were measured using Wako Diagnostics NEFA-HR kit (999-34691, 995-34791, 991-34891, 993-35191).

2.4. Mitochondrial respirometry and fatty acid oxidation

Respirometry was performed using an Oroboros O_2K High-Resolution Respirometer using mitochondrially-enriched liver samples prepared as described above. Respiration was measured in MiR05 buffer at 37 °C under constant mixing in a sealed, 2-ml chamber. The respirometry protocol consisted of sequential additions of substrates and inhibitors as follows: pyruvate (5 mM), malate (2 mM), and glutamate (10 mM); adenosine diphosphate (ADP, 2 mM); oligomycin (2.5 μM); carbonyl cyanide 4-(trifluoromethoxy)phenylhydrazone (FCCP; titrations of 0.5 μM until maximal respiration reached); and antimycin A (2.5 μM). Protein concentration of the mitochondrially enriched fraction was determined by BCA protein assay, and oxygen consumption or flux was expressed per mg protein. The respiratory control ratio (RCR) was calculated as the ratio of ADP-stimulated relative to oligomycin-stimulated states. The coupling control ratio (CCR) was calculated as the ratio of routine relative to ADP-stimulated states, where routine respiration represents oxygen consumption in the presence of substrates (pyruvate, malate, glutamate) prior to ADP addition [33]. The flux control ratio for complex I-mediated oxidative phosphorylation relative to maximal electron transport chain (ETC) capacity (P_I/E) was calculated as the ratio of ADP-stimulated relative to FCCP-stimulated states. Respiration dedicated to oxidative phosphorylation (OXPHOS) was calculated as the difference between ADP-stimulated and oligomycin-stimulated states. Leak respiration was calculated as the difference between oligomycin-stimulated and antimycin A-stimulated states.

Fatty acid oxidation rates were measured using mitochondrially enriched liver samples prepared as above in STE buffer. Samples were incubated at 37 °C for 180 min in triplicate in oxidation buffer (100 mM sucrose, 10 mM Tris—HCl, pH 7.4, 5 mM KH_2PO_4, 0.2 mM EDTA, 80 mM KCl, 1 mM $MgCl_2$, 2 mM L-carnitine, 0.1 mM malate, 0.05 mM coenzyme A, 2 mM ATP, 1 mM DTT) in the presence of BSA-conjugated oleic acid (0.25 mM) and 0.5 μCi 1-^{14}C-oleic acid (Perkin Elmer) in a sealed reaction chamber, followed by acidification of the reaction mixture and capture of $^{14}CO_2$ for calculation of fatty acid oxidation rates.

2.5. Histology

Preparation and staining of all histological samples were conducted at the University of Pittsburgh Department of Pathology in the Pitt Biospecimen Core. The left lobe of the liver was excised from each mouse at the time of dissection and fixed in 4% formalin overnight, washed, and then transferred to 70% ethanol diluted in phosphate-buffered saline (PBS). Samples were then embedded in paraffin for sectioning and subsequent staining with hematoxylin and eosin (H&E) for analysis. The NAFLD activity score (NAS) was made based on methods established by the Pathology Committee of the Non-alcoholic Steatohepatitis (NASH) Clinical Research Network [34]. NAS was determined in a blinded fashion by two individuals, and the scores were averaged. NAS consisted of separate category scores made in whole-value increments for steatosis (0-3), where 0 = 0—5%, 1 = 6—33%, 2 = 34—66%, and 3 = 67—100% of hepatocytes positive for steatosis; inflammation (0-3), where 0 = no foci, 1 = more than 2 foci per 200X field, 2 = 2-4 foci per 200X field and 3 = greater than 4 foci per 200X field; and ballooning (0-2), where 0 = none present, 1 = few and 2 = many/prominent. The final NAS represents a sum of the three category scores.

2.6. Hyperinsulinemic-euglycemic clamps

Clamp studies were performed as previously described [31] with minor modifications. Briefly, mice underwent surgery to implant an indwelling catheter in the right jugular vein and recovered five days prior to study. Mice were fasted six hours in the morning prior to study. Basal (fasted) and insulin-stimulated (clamp) rates of glucose turnover (whole-body glucose uptake and endogenous or hepatic glucose production) were measured by isotope dilution using a primed/continuous infusion of 3-^{3}H-glucose (Perkin Elmer; prime: 0.7 μCi/kg over 3 min; 0.05 μCi/min basal, 0.1 μCi/min clamp). Insulin was given as a primed/continuous infusion (Novolin-R, Novo Nordisk; prime dose: 30 mU/kg over 3 min; continuous dose: 4.5 $mU \cdot kg^{-1} \cdot min^{-1}$). Plasma glucose levels were checked using blood collected by tail vein massage every 10 min during study, and euglycemia was maintained with a variable infusion of 20% dextrose.

2.7. Genetic analyses

For RNA-seq studies, RNA was isolated from flash-frozen pulverized liver using TRI reagent and Qiagen RNeasy columns per the manufacturer's instructions. Library construction and sequencing were performed by Novogene, as previously described (Zhu, Circ Res, 2019). Briefly, a paired-end cDNA library was constructed and sequenced using the Illumina NovaSeq 6000 platform, consisting of paired-end 150 base pair reads. Sequencing reads were mapped to the mouse reference genome (mm10) using the Spliced Transcripts Alignment to a Reference (STAR) aligner, followed by quantification of gene expression level or fragments per kilobase of transcript per million mapped reads (FPKM) using HTSeq. Differentially expressed genes between comparison groups were identified using the DESeq2 R package, and resulting P-values were adjusted to control for false discovery rate. An adjusted P-value less than 0.05 was considered significant. Additional analyses, including gene ontology (GO) and Kyoto Encyclopedia of Genes and Genomes (KEGG) enrichment, were performed using the clusterProfiler R package.

For quantitative polymerase chain reaction (qPCR) studies to confirm RNA-seq data, RNA was extracted using the RNeasy Kit, as above, followed by cDNA synthesis, including DNase pre-treatment, using QuantiTect Reverse Transcriptase Kit (Qiagen). QPCR was performed using the Applied Biosystems QuantStudio3 RT-PCR System and PowerUp SYBR Green Master Mix (Thermo Fisher). Primer sequences were designed with the IDT Real-Time PCR tool or purchased from Qiagen (*Cd36* QT01058253). Sequences for commercial primers are proprietary. Sequences for designed primers were as follows: *Acot2* (F CCCCAAGAGCATAGAAACCAT; R CATAGCAAGGCCAAGTTCAC); *Actb* (F GCAGCTCCTTCGTTGCCGGT; R TACAGCCCGGGGAGCATCGT); *Apoa4* (F GAA GACGGATGTCACTCAG; R CTTCACCCTCTCAGTTTCCTG); *B2m* (F GGTCGCTTCAGTCGTCAG R TTCAGTATGTTCGGCTTCCC); *Cidec* (F AGATCGGAAGGTTCGCAAAG; R ACGATTGTGC CATCTTCCTC); *Col1a1* (F CATAAAGGGTCATCGTGGCT; R TTGAGTCCGTCTTTGCCAG); *Col1a2* (F AAGGATACAGTGGATTGCAGG; R TCTACCATCTTTGCCAACGG); *Col3a1* (F GAAGTCTC TGAAGCTGATGGG; R TTGCCTTGCGTGTTTGATATTC); *Col5a2* (F CAAACTGGAGGT GGAGATACTAG; R CTCTTGGTCCTTGTGATCCTG); *Cyp1a2* (F AGCACAGCGAGAACTACAAAG; R ACGTTAGGCCATGTCACAAG); *Cyp2b13* (F GCTTTTCTACCCTTCTCCACAG; R ATG TCCTTAGAAGCAACAGGG); *Cyp2b9* (F CCTCGACTACATTGCCCATAG; R TTCTGGTGATGG AACTCTGTG); *Cyp2c29* (F TCAGCCAATCCTTCACCAAC; R CTTCCTCTACCAGCAAACTCC); *Cyp2c37* (F GATATGCTCTCCTACTCCTGTTG; R GCCGATCACATGCTCAATTTC); *Cyp2c50* (F GATATGCTCTCCTACTCCTGTTG; R GCCGATCACATGCTCAATTTC); *Cyp2c54* (F AACCCAGAGA AGTTTGACCC; R TGGTTAGGAACAGGAACAGC); *Cyp4a14* (F GAAGGCCAGGAAGAAGAGACAC; R GTGGCCAGAGCATAGAAAATCC); *Foxq1* (F ACTCGCTTCCTACGACCTC; R CGAACACCTCCA ATTTCATGC); *Gapdh* (F AGGTCGGTGTGAACGGATTTG; R TGTAGACCATGTAGTTGAGGTCA); *Gpat3* (F CCATCTATCCAGTGGCCATAAAG; R CGAAGCAGGTAGCTCACCAAGT); *Gsta1* (F GGGTGGAGTTTGAAGAGAAGT; R TGGCGATGTAGTTGAGAATGG); *His1h2bq* (F TTGCTTGAGTT TGCACGGCT; R ACAGGCGGTGATGACACTCG); *Lamb3* (F ACGGCTTCTCATCCAACAG; R CCTGGATCTCTTTCATCTTGCG); *Myc* (F AGGCCCCCAAGGTAGTGATC; R GTGCTCGTCT GCTTGAATGG); *Pck1* (F GTCACCATCACTTCCTGGAAGA; R GGTGCAGAATCGCGAGTTG); *Pdk4* (F TGGACCCCGTTACCAATCAA; R CCACATCACAGTTTGGGTCG); *Socs3* (F CCTATGAGAA AGTGACCCAGC; R TTTGTGCTTGTGCCATGTG); *Thbs1* (F ACTTCACCTTTGCCACCTC; R AGACTCTGGAATGCGGTTG); *Tnc* (F ATAGCCAACATCACAGACTCAG; R GCTCGTACTCCA CTGTATTTCC). The efficiency of each primer pair was determined from a four-point standard curve and used to calculate relative expression using a housekeeping gene, as noted, and final data is expressed as fold-change in relative expression comparing LKO to WT mice for each diet.

For mitochondrial DNA (mtDNA) copy number measures, total tissue DNA was isolated from snap frozen samples in ProK buffer (XyZ) and lightly dounced to increase surface area and extraction efficiency before digesting overnight at 55 °C. The samples were processed as previously described [35]. DNA was resuspended in water, quantitated for dsDNA content, and diluted to 1 ng/μL. Nuclear DNA and mtDNA were quantitated from each sample using *Tbp* and *Nd1* duplex TAQMAN assays, respectively, as previously described [36], using the $\Delta\Delta$Cq method [37]. A standard curve was generated using equal parts of all samples and serial dilution to ensure linearity of each TAQMAN assay. The relative abundance of mtDNA was normalized to the standard curve. The average of technical triplicates was recorded for each animal, then grouping was revealed.

2.8. Hepatic lipid secretion

Mice were transferred to clean cages the evening prior to study and fasted overnight to ensure that intestinal contents were depleted. The following morning, a fasted plasma sample was collected by tail bleed, followed by intraperitoneal injection of poloxamer 407 (1 g/kg body weight) to inhibit tissue lipoprotein lipase activity [38]. Plasma samples were collected at 30, 60, 120, and 240 min after dosing. Plasma triglyceride levels were measured as described above, and the rate of hepatic lipid secretion calculated as the change in plasma triglyceride levels from 0 to 30 min and 30—240 min.

2.9. Metabolic cage studies

The major determinants of energy balance were measured in the Columbus Labs Animal Monitoring System, including feeding, activity, and energy expenditure, by indirect calorimetry and respiratory exchange ratio. Mice were individually housed during metabolic cage studies. Studies consisted of 72 h of cage time where the first 24 h was considered acclimation and the subsequent 48 h was used to calculate the 24-hour and 12-hour light and dark cycle averages for each parameter measured. HFD-fed mice were studied in metabolic cages after 3 weeks of HFD feeding.

2.10. Statistical analyses

Studies were designed and performed to test the effect of liver-specific deletion of *Prkn* on multiple endpoints. The effect of *Prkn* deletion was evaluated under RC and HFD conditions separately. RC and HFD data are shown together for ease of presentation and not to imply comparisons between all groups (i.e., interactions or effects of diet). Data shown are the mean ± standard error of the mean. Data were compared by Student's t-test, where $P < 0.05$ was considered significant. Details of statistics pertaining to RNA-seq are described above in Methods section 2.7.

3. RESULTS

3.1. Generation of liver-specific *Prkn* knockout mice

Based on limitations of the whole-body *Prkn* knockout line for understanding the role of *Prkn* in specific tissues, we generated a conditional (floxed) transgenic *Prkn* mouse using CRISPR-Cas9 genetic editing [39]. C57BL/6J zygotes were co-injected with *Cas9* mRNA, single-guide RNAs designed to create double-strand breaks flanking exon seven of *Prkn* (Figure 1A), and targeted inserts were designed to include the loxP sequence and homology to the *Prkn* sequence flanking the double strand breaks. We identified founders by PCR (Figure 1B), where presence of the 5′ and 3′ loxP sites were detected as approximate 25 base pair shifts and confirmed proper insertion by sequencing. Exon seven encodes the RING1 domain of *Prkn* and is essential for PARKIN E3 ligase activity [40]. Homozygous *Prkn* exon seven flox mice were crossed to the well-characterized B6.Cg-Tg(Alb-cre)21Mgn/J mice purchased from Jackson Labs (strain #003574) to produce LKO and littermate WT controls. Tissue-specific deletion of PARKIN protein was confirmed by immunoblot using lysates from the heart, kidney, liver, and skeletal muscle (Figure 1C), as well as white adipose and small intestine (data not shown).

3.2. Diet-induced hepatic steatosis is exacerbated in liver-specific *Prkn* knockout mice

Previous reports in whole-body *Prkn* knockout mice demonstrated a clear role for PARKIN in the regulation of body weight and adiposity, particularly during HFD feeding [14,29,31]. To determine whether

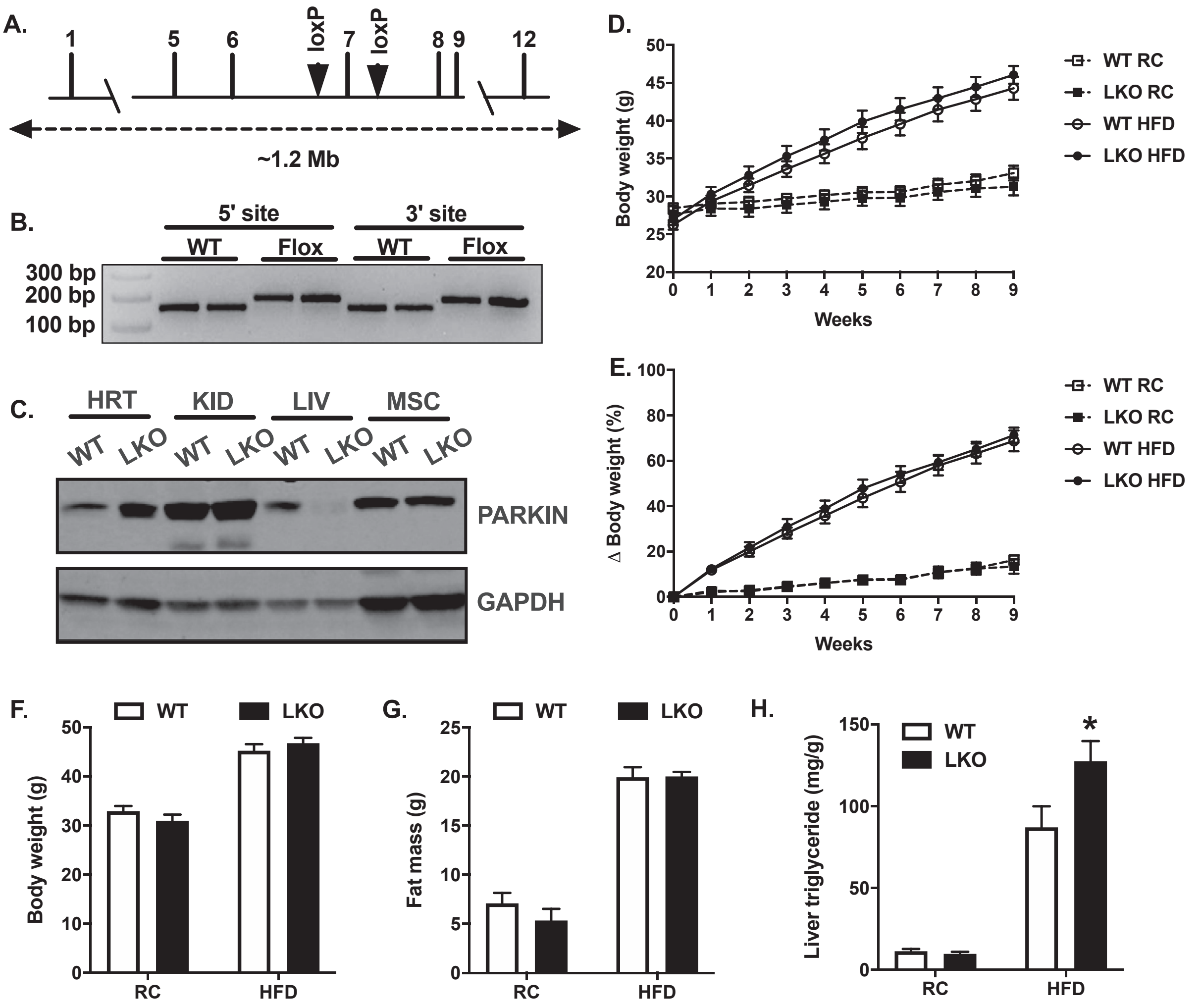

Figure 1: Hepatic steatosis is increased in high-fat diet fed liver-specific *Prkn* knockout mice. A. Targeting strategy for loxP insertions flanking exon seven of *Prkn*. **B.** PCR confirmation of 5′ and 3′ loxP insertions by CRISPR-Cas9 genetic editing of C57BL6J zygotes. **C.** Western blots confirming tissue-specific deletion of PARKIN after backcrossing *Prkn*$^{fl/fl}$ mice to Albumin-Cre mice. **D.** Changes in body weight over nine weeks during regular chow (RC) and high-fat diet (HFD) studies. **E.** Changes in body weight in percent relative to baseline over nine weeks during RC and HFD studies. **F.** Final body weights at the end of RC and HFD studies. **G.** Final body fat measured by ^{1}H-NMR. **H.** Liver triglyceride levels. Data are the mean ± S.E.M. for n = 8–12 mice per group. The effect of genotype was compared by Student's t-test, where $^*P < 0.05$.

hepatic PARKIN contributed to the reduced body weight and adiposity observed in whole-body knockouts in previous studies, we measured changes in body weight over a nine-week period during both RC and HFD feeding. There were no differences in body weight (Figure 1D) or body weight gain between WT and LKO mice on either RC or HFD, in which both genotypes gained approximately four grams during RC feeding and 18.5 g during HFD feeding (Supplemental Fig. 1A), or increases of 15% and 70%, respectively, on each diet (Figure 1E). Final body weights and whole-body adiposity and lean mass were also similar between genotypes on each diet (Figure 1F—G; Supplemental Fig. S1B), demonstrating that hepatic PARKIN does not contribute to previously reported differences in body weight in whole-body *Prkn* knockout mice. As expected, based on the lack of differences in body weight, there were no differences in energy expenditure, respiratory exchange ratio, feeding, or activity between genotypes on RC or HFD during metabolic cage studies (Supplemental Fig. S2A-H).

HFD-fed whole-body *Prkn* knockout mice were also previously shown to be protected from diet-induced hepatic steatosis [29,30]. While there were no differences in liver triglyceride levels between WT and LKO mice fed RC (Figure 1H), hepatic steatosis was significantly increased by 45% in HFD-fed LKO compared with HFD-fed WT mice (Figure 1H). Histological evaluation demonstrated that liver fat in HFD-fed LKO mice consisted of both micro- and macrovesicular steatosis compared with primarily microvesicular steatosis in HFD-fed WT mice (Figure 2A). Steatosis also appeared limited to hepatic zones two and three in HFD-fed WT mice, whereas steatosis was widespread and evident in zones one, two, and three in HFD-fed LKO mice. Histological scoring for steatosis performed in a blinded fashion by two individuals confirmed significantly increased liver fat in HFD-fed LKO compared with HFD-fed WT mice, as well as no difference between genotypes on RC (Figure 2B). Hepatocyte ballooning, which was rare in all samples, appeared modestly increased in HFD-fed LKO compared with HFD-fed WT mice, although the difference was not significant (Figure 2C). Lobular inflammation was also a low-frequency event in all samples, and there were no differences between genotypes on either diet (Figure 2D). Lastly, the NAFLD activity score or NAS was significantly

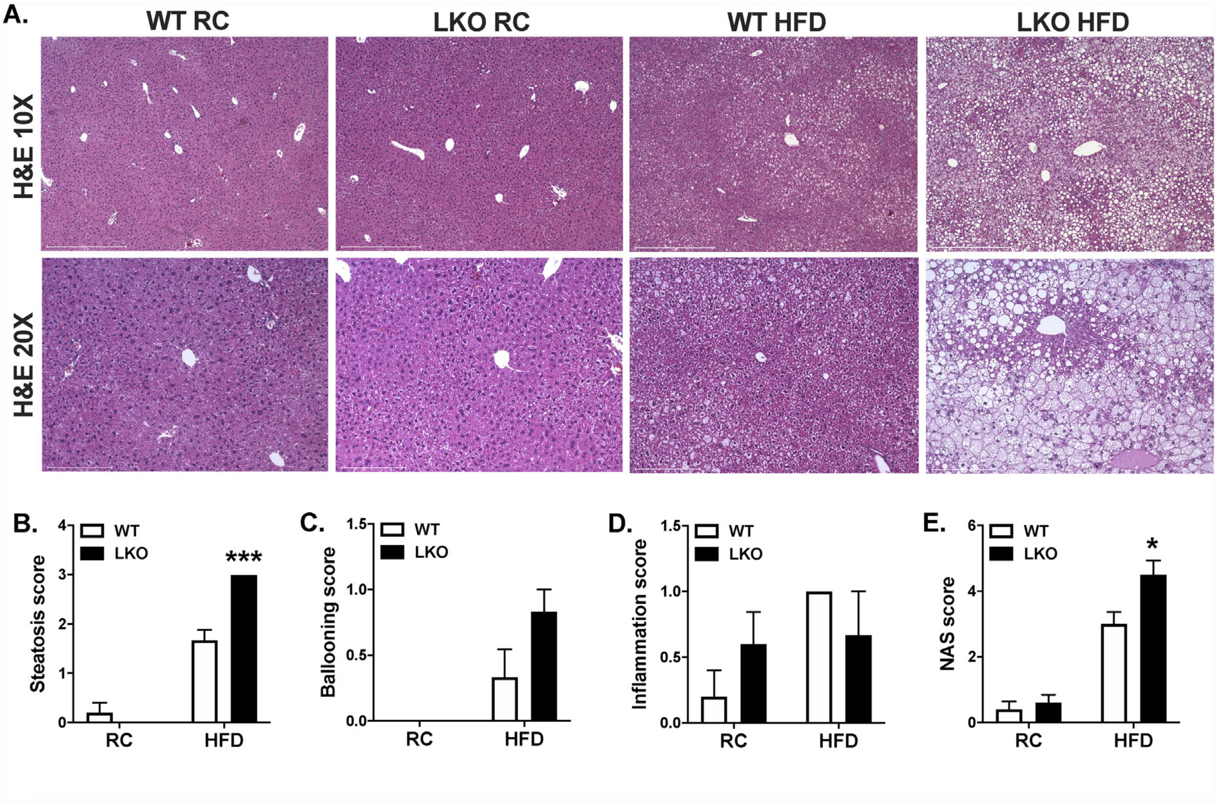

Figure 2: **NAFLD activity score is increased in high-fat diet fed liver-specific *Prkn* knockout mice. A.** Representative images of H&E stained sections. **B.** Histological scores for steatosis ranging from 0 to 3 made in whole-value increments, where 0 = 0–5%, 1 = 6–33%, 2 = 34–66%, and 3 = 67–100% of hepatocytes positive for steatosis; **C.** hepatocyte ballooning ranging from 0 to 2, where 0 = none present, 1 = few, and 2 = many/prominent; and **D.** lobular inflammation ranging from 0 to 3, where 0 = no foci, 1 = more than 2 foci per 200X field, 2 = 2-4 foci per 200X field and 3 = greater than 4 foci per 200X field. **E.** Composite NAFLD activity score (NAS) reflecting sum of scores in B-D. Data are the mean ± S.E.M. for n = 5–6 mice per group. The effect of genotype was compared by Student's t-test, where *P < 0.05.

increased in HFD-fed LKO compared with HFD-fed WT mice, largely reflecting the significant increase in hepatic steatosis (Figure 2E).

3.3. Genetic markers of *NAFLD* progression are enhanced in the absence of hepatic *Prkn*

To gain an unbiased understanding of the genetic changes that occurred following liver-specific *Prkn* knockout, we performed global gene expression analysis of liver samples by RNA-seq, comparing WT and LKO mice on RC and HFD. When comparing LKO and WT mice fed RC, we detected only ten significant, differentially expressed genes between genotypes, where nine genes were upregulated (*Phlda1, Cxcl14, Myc, Cish, Foxq1, Socs3, Histh2bq, Mup15 and Mup16*) and one gene was suppressed (*Cyp4a14*) in LKO compared with WT mice (Figure 3A). Gene-annotation analysis to infer enriched pathways, processes, or functions within the differentially expressed genes primarily suggested significant changes within the JAK-STAT signaling pathway (*Myc, Cish, Socs3*) and negative regulation of the insulin receptor signaling cascade (*Cish, Socs3*), and to a lesser extent changes in transcriptional regulation (*Myc, Foxq1*) and ubiquitin-like protein ligase binding (*Myc, Hist1h2bq*; Figure 3B).

In contrast to the small number of differentially expressed genes in the RC-fed comparison, there were 113 significant, differentially expressed genes when comparing HFD-fed mice, where 82 genes were upregulated and 31 genes downregulated in LKO compared with WT mice (Figure 3C). Gene annotation analysis for KEGG pathway enrichments demonstrated significant changes in lipid and metabolic pathways, as well as pathways suggesting fibrosis (Figure 3D). GO analysis identified similar enrichments in metabolic and extracellular matrix pathways classified within biological processes (BPs), cellular component (CCs), and molecular function (MF) pathways (Figure 3E). Across both gene annotation analyses, enrichments in metabolic pathways were largely driven by significant changes in genes regulating lipid metabolism (*Acot2, Elovl5, Ces3, Hsd3b5, Apoa4, Cd36, Cidea, Cidec, Mogat1, Gpat3, Scd1*), carbohydrate metabolism (*Pck1, Pdk4*), belonging to the cytochrome P450 gene family (*Cyp1a2, Cyp2b9, Cyp2b13, Cyp2c29, Cyp2c37, Cyp2c50, Cyp2c54*) or glutathione S-transferase family (*Gsta1, Gstm3*). Enrichments in pathways suggesting fibrosis within each annotation analysis were driven by significant changes in genes in the collagen and laminin family (*Col1a1, Col1a2, Col3a1, Col4a1, Col5a2, Lamb3*), annexin family (*Anxa2, Anxa5*), or encoding glycoproteins involved in cell—cell or cell—matrix interactions (*Thbs1, Tnc*). Key genes for each of the above pathways in RC (Figure 3F) and HFD (Figure 3G—H) samples were confirmed by quantitative PCR. Complete lists of differentially expressed genes and gene-annotation analyses are available within the supplemental materials.

Hepatic steatosis and fibrosis are frequently associated with changes in plasma lipid and liver enzyme levels [41,42]. Consistent with the lack of change in liver fat or large-scale changes in hepatic gene expression, we found no differences between RC-fed LKO or RC-fed WT mice when comparing plasma lipid levels, including fatty acids, cholesterol, and triglycerides, nor in plasma liver enzyme levels,

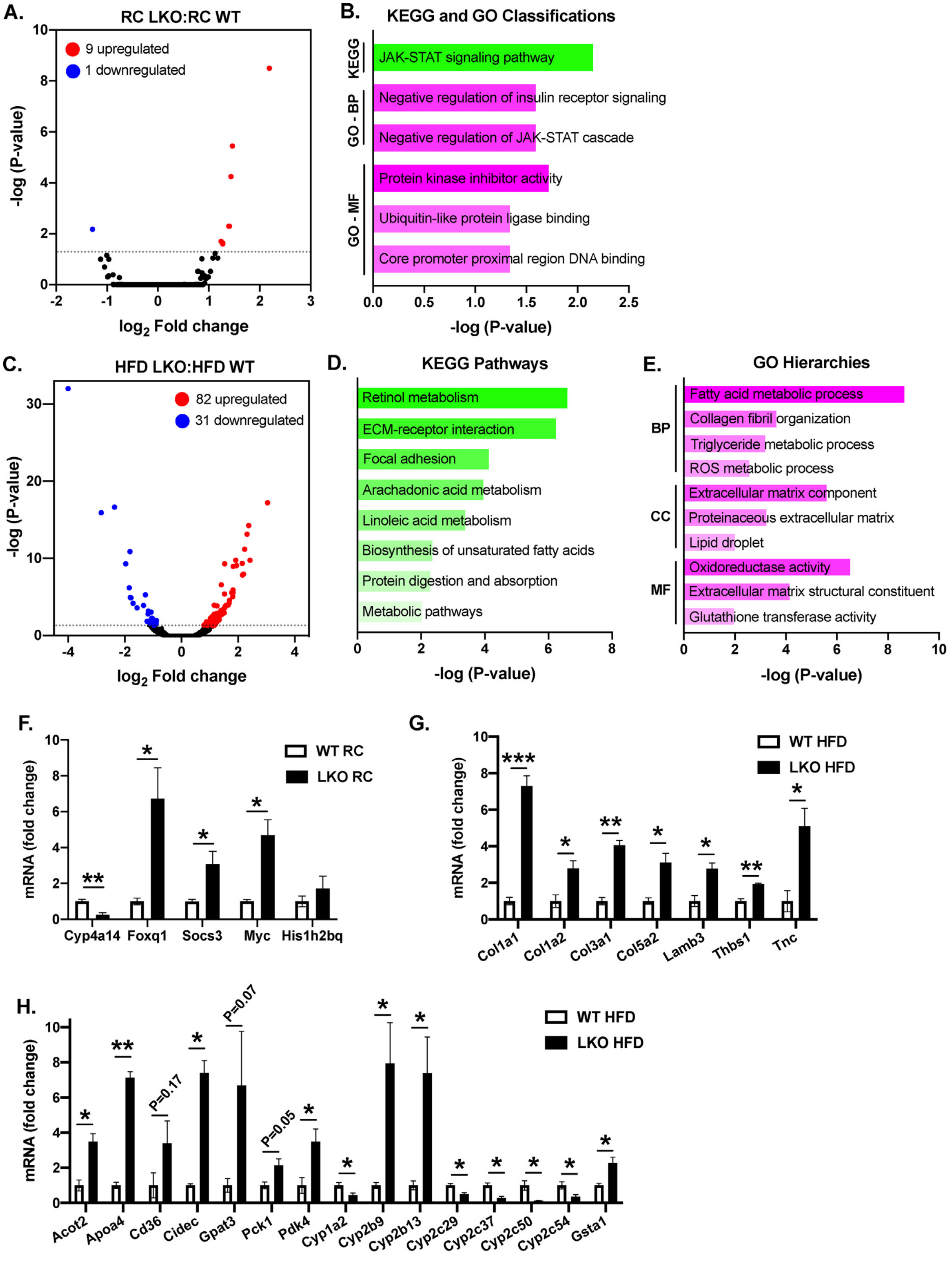

Figure 3: Liver-specific deletion of *Prkn* exacerbates changes in gene expression associated with NAFLD progression. A. Volcano plot of RNA-seq data comparing RC-fed LKO with WT mice. **B.** Gene annotation summary for enriched pathways detected by KEGG and GO analyses. **C.** Volcano plot of RNA-seq data comparing HFD-fed LKO with WT mice. **D.** Gene annotation summary for enriched pathways detected by KEGG and **E.** GO analyses. Abbreviations: BP = biological process; CC = cellular component; MF = molecular function. Data in A and C represent the $\log_2$ fold change in gene expression of LKO compared with WT, as well as the negative log of the adjusted P-value for the entire RNAseq dataset. F. Quantitative PCR for the indicated target genes for RC-fed mice. **G-H.** Quantitative PCR for the indicated target genes organized by pathway (G: fibrosis; H. metabolism) for HFD-fed mice. Data in F–H are expressed as fold-change in expression relative to WT following calculation of relative expression using a housekeeping gene (*Actin, Gapdh, B2m*) and individual primer efficiencies determined at the time of study. Data are the mean ± S.E.M. for n = 3 mice per group and were compared by Student's t-test, where $^*P < 0.05$, $^{**}P < 0.01$, and $^{***}P < 0.001$.

including aspartate aminotransferase (AST) and alanine aminotransferase (ALT; Table 1). Similarly, plasma fatty acid and cholesterol levels were not different when comparing HFD-fed LKO and HFD-fed WT mice; however, plasma triglycerides were significantly reduced by 23% in LKO mice (Table 1). We measured rates of hepatic triglyceride secretion *in vivo*, but found no differences between genotypes, suggesting that reduced liver lipid export did not contribute to the reduced plasma triglyceride levels and increased steatosis (Supplemental Fig. S3). In contrast to RC-fed mice, plasma AST and ALT levels were 1.3- and 2.8-fold greater in HFD-fed LKO compared with HFD-fed WT mice ($P < 0.05$; $P = 0.09$; Table 1).

3.4. Mitochondrial respiratory capacity is impaired in liver-specific *Prkn* knockout mice

Next, we evaluated the effects of *Prkn* deletion on multiple, static markers of mitochondrial content in the liver from WT and LKO mice. Protein expression of mitochondrial electron transport chain complex proteins NADH:ubiquinone oxidoreductase subunit B8 (NDUFB8; complex I), succinate dehydrogenase iron-sulfur subunit (SDHB; complex II), ubiquinol-cytochrome C reductase core protein 2 (UQCRC2; CIII) and cytochrome C oxidase subunit I (MTCO1; CIV), as well as ATP synthase F1 subunit alpha (ATP5A), were similar between WT and LKO mice on RC and HFD (Figure 4A). We also found no differences in mitochondrial DNA copy number or citrate synthase activity between genotypes on either diet (Figure 4B—C), and protein levels of common mitochondrial markers voltage-dependent anion-selective channel protein (VDAC), heat shock protein 60 (HSP60), succinate dehydrogenase flavoprotein subunit (SDHA), and prohibitin-1 (PHB1) were also unchanged in LKO compared with WT mice on RC or HFD (Figure 4D). These data demonstrate that hepatic mitochondrial content was unaffected by the loss of PARKIN.

To determine the effects of liver-specific deletion of *Prkn* on hepatic mitochondrial respiratory function, we measured oxygen consumption from mitochondrial-enriched fractions from liver using high-resolution respirometry on the Oroboros O_2K platform. The respiratory control ratio (RCR), reflecting the ratio of state 3 to state 4° respiration, serves as a robust overall measure of mitochondrial function, as it integrates the key components of oxidative phosphorylation, including substrate oxidation, ATP turnover, and uncoupling [43]. The RCR was reduced by 20% in RC-fed LKO compared with RC-fed WT mice, while there were no differences between genotypes on HFD (Figure 5A; $P < 0.05$). Similar to results for RCR, the coupling control ratio (CCR), which serves as an index of uncoupling [33], was increased by 20% in RC-fed LKO compared with RC-fed WT mice, while there were no differences between genotypes on HFD (Figure 5B; $P < 0.05$). Additionally, the flux control ratio for oxidative phosphorylation (P_I/E), where state 3 respiration in the presence of NADH-linked or complex I substrates is expressed relative to the uncoupled state or maximal capacity of the electron transport system, was reduced by 15% in LKO compared with WT mice during RC feeding, while there were no differences between groups fed HFD (Figure 5C; $P < 0.05$). To understand what aspects of mitochondrial respiratory function contributed to the changes in flux control ratios in RC-fed mice, we compared absolute rates of respiratory capacity between groups. Mitochondrial respiratory capacity in support of oxidative phosphorylation (OXPHOS) was reduced by 24% in RC-fed LKO compared to RC-fed WT mice (Figure 5D; $P < 0.05$), while there were no differences in the leak respiration or the maximal capacity of the ETS (Figure 5E—F). Mitochondrial fatty acid oxidation, measured as the production of ^{14}C-labeled CO_2 following incubation of mitochondrially enriched liver fractions with ^{14}C-oleate, was reduced by 40% in RC LKO compared with RC WT mice ($P < 0.01$; Supplemental Fig. S3). Consistent with the lack of changes in flux control ratios in HFD-fed mice, there were no differences in absolute rates of respiration between genotypes following HFD-feeding (Figure 5D—F). Together, these data demonstrate that liver mitochondrial respiratory capacity is impaired in the absence of PARKIN, and suggest that a defect or defects in systems that support oxidative phosphorylation, namely substrate oxidation and ATP turnover, account for the observed changes.

Table 1 — Plasma biochemistry from WT and LKO male mice fed RC and HFD. Data are the mean ± S.E.M. for 5-6 mice per group. Data analyzed by Student's t-test comparing WT to LKO within each dietary group. *$P < 0.05$.

	WT RC	LKO RC	WT HFD	LKO HFD
Fatty acids (mM)	0.463 ± 0.020	0.485 ± 0.052	0.458 ± 0.043	0.397 ± 0.037
Cholesterol (mg/dl)	80.7 ± 8.5	80.9 ± 4.2	191 ± 10	203 ± 23
Triglyceride (mg/dl)	59.6 ± 13.2	59.9 ± 6.9	42.1 ± 3.5	32.6 ± 2.1*
AST (U/L)	28.0 ± 4.2	23.9 ± 2.2	167 ± 17	224 ± 16*
ALT (U/L)	21.0 ± 6.3	14.2 ± 1.6	97.0 ± 30.8	277 ± 91

3.5. Insulin sensitivity is reduced in HFD-fed liver-specific Prkn knockout mice

Hepatic steatosis is strongly associated with insulin resistance [44], and insulin resistance is thought to contribute to the pathogenesis of NAFLD [5]. Based on the increased liver fat and markers of NAFLD in HFD-fed LKO mice, we evaluated insulin resistance in HFD-fed mice using hyperinsulinemic euglycemic clamps. Fasting plasma glucose levels were 10% greater in LKO compared with WT mice (Figure 6A; $P = 0.09$) and there were no differences in fasting rates of endogenous or hepatic glucose production (EGP) between groups (Figure 6B). There were also no differences in fasting (basal) plasma insulin levels between groups, and plasma insulin levels were matched during the hyperinsulinemic euglycemic clamp (Figure 6C). During the 120-min hyperinsulinemic infusion, plasma glucose levels were matched between groups at approximately 155 mg/dL, reflecting euglycemic or fasting levels (Figure 6D). The glucose infusion rate (GIR) required to maintain euglycemia in the LKO mice was 35% less than that required for WT mice (Figure 6E—F; $P < 0.05$), demonstrating impaired whole-body insulin sensitivity or increased insulin resistance in HFD-fed LKO mice. The impaired whole-body insulin sensitivity was due to modest, non-significant changes in both glucose uptake (Figure 6G; $P = 0.38$) and impaired suppression of hepatic glucose production by insulin (Figure 6H; $P = 0.11$). Phosphorylation of Akt in post-clamp liver lysates was significantly reduced in LKO compared with WT mice, demonstrating impaired insulin signaling (Figure 6I—J; $P < 0.05$). Overall, there was a 5.3 $mg \cdot kg^{-1} \cdot min^{-1}$ difference in insulin sensitivity between groups, reflected as the difference in GIR (Figure 6E—F; $P < 0.05$), which was accounted for by a 3.3 $mg \cdot kg^{-1} \cdot min^{-1}$ increase in EGP and a 2.0 $mg \cdot kg^{-1} \cdot min^{-1}$ reduction in whole-body glucose disposal. Thus, reduced hepatic insulin sensitivity accounted for 60% or the majority of the increased whole-body insulin resistance in LKO mice compared with changes in glucose uptake, which accounted for 40% of the overall effect.

4. DISCUSSION

The primary goal of these studies was to determine the physiological effects of liver-specific *Prkn* deletion, specifically with regard to the effects on mitochondrial respiratory capacity, hepatic steatosis, and

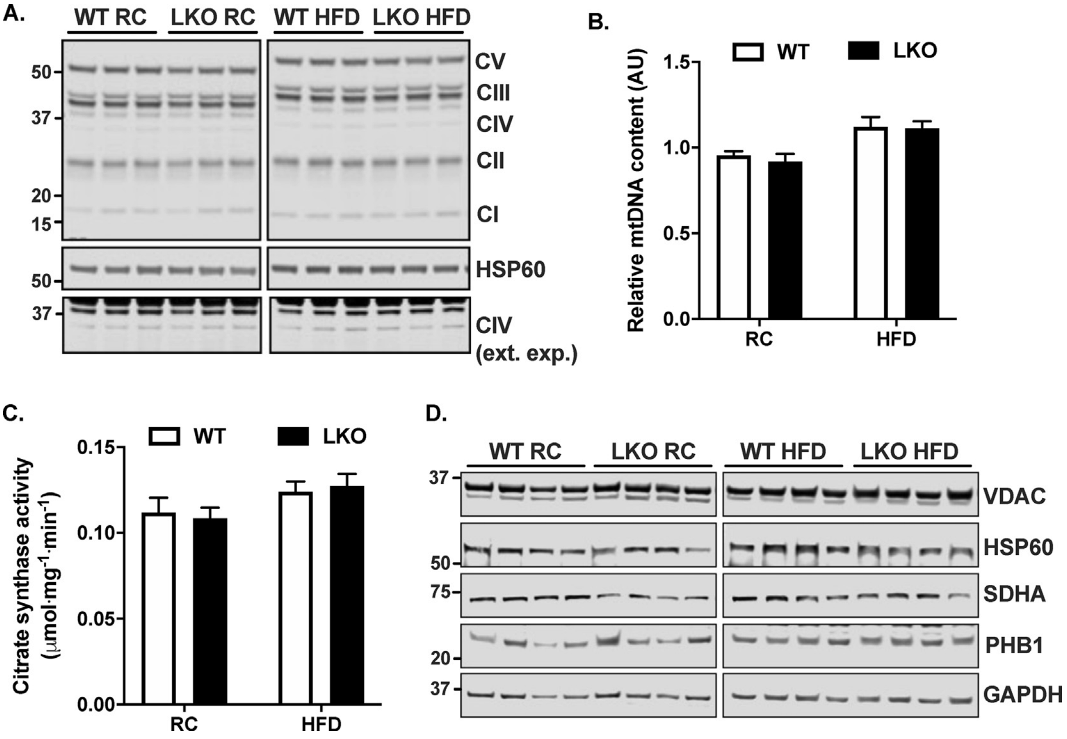

Figure 4: Deletion of hepatic *Prkn* does not affect markers of mitochondrial mass. A. Western blot from liver lysates for electron transport chain respiratory complex proteins CI—CIV and the ATP synthase (CV), as well as HSP60 loading control. Lower blot shows an extended exposure for CIV marker MTCO1, which appeared faintly in upper blot. **B.** Liver mitochondrial DNA content measured by PCR. **C.** Citrate synthase activity measured in liver lysates. **D.** Western blots from liver lysates for markers of mitochondrial mass. Data are the mean ± S.E.M. for n = 5—6 mice per group.

insulin resistance. We found that in contrast to whole-body *Prkn* knockout mice [29,31], LKO mice were not protected from diet-induced obesity and were thus a valid model to evaluate the role of PARKIN in liver in response to nutritional stress without confounding differences in body weight. We also found that LKO mice developed more severe steatosis during HFD feeding and that markers of NAFLD progression, including NAFLD activity score and changes in fibrotic gene expression, and plasma liver enzymes were more markedly induced in LKO compared with WT mice. Additionally, HFD-fed LKO mice were more insulin-resistant compared with WT mice, and changes in liver insulin responsiveness accounted for the majority of the whole-body insulin resistance. These observations demonstrate that hepatic PARKIN plays a protective role against metabolic dysfunction in liver during over nutrition and suggest that loss of PARKIN-mediated mitophagy in the liver may hasten the onset of obesity-associated NAFLD.

The observed effects of liver-specific *Prkn* deletion on hepatic steatosis in our study may result from multiple mechanisms. Based on the evidence presented, it is unlikely that changes in whole-body energy balance (feeding, activity, or energy expenditure) or alterations in mitochondrial content contributed to the phenotype. Alternatively, changes in mitochondrial quality may drive the observed phenotype. The reduced respiratory capacity observed in RC-fed LKO mice may predispose them to steatosis during HFD feeding due to an inability to buffer the increased metabolic substrate supply through increased oxidation. Additionally, the impaired mitochondrial efficiency observed in LKO mice may result in excessive but incomplete oxidation of lipids during HFD feeding. In this model, an increased supply of triglycerides or fatty acids to meet the energetic demands of the hepatocyte due to the loss of mitochondrial efficiency exceeds rates of utilization, such that steatosis develops gradually over time. An increased supply to and uptake of lipids by the liver during HFD feeding may also explain the unaccounted-for reduction in plasma triglyceride levels in the LKO mice. Both the increased steatosis and increased mitochondrial inefficiency then likely contributed to the development of insulin resistance and progression of NAFLD. Hepatic insulin resistance is strongly associated with steatosis, in which increased levels of lipid species, such as diacylglycerols and ceramide, activate stress signaling cascades that inhibit the insulin receptor signaling pathway [45,46]. Impaired mitochondrial respiratory efficiency is commonly associated with increased reactive oxygen species production and is positively associated with insulin resistance, inflammation, and the pathogenesis of NAFLD [11,47,48].

Our data on the effects of liver-specific deletion of *Prkn* on mitochondrial respiratory function are consistent with several previous reports in whole-body *Prkn* knockout mice, which demonstrated impaired mitochondrial respiration in multiple tissue types, including the ventral midbrain, skeletal muscle and heart [14,27,49]. As in our experiments, each of these studies reported reduced mitochondrial respiratory capacity during ADP-stimulated respiration (OXPHOS) in the presence of complex I or NADH-linked substrates [14,27,49]. We also detected changes in mitochondrial efficiency suggestive of uncoupling, namely reduced RCR and increased CCR in LKO mice. Similar reductions in mitochondrial efficiency were reported in skeletal muscle, but not ventral midbrain of *Prkn* knockout mice, and no report of coupling control ratios was made for heart [14,49]. Reports on the effects of whole-body *Prkn* knockout on liver mitochondrial function have been less conclusive, reporting no differences in mitochondrial

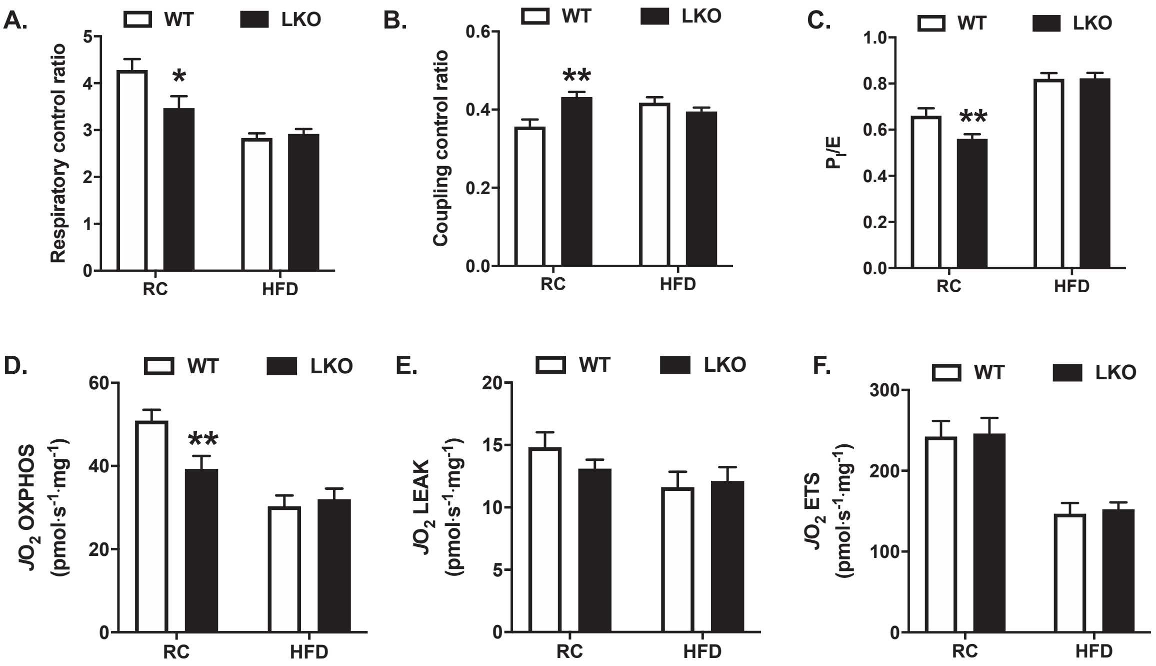

Figure 5: Hepatic mitochondrial respiratory capacity is impaired in liver-specific *Prkn* knockout mice. A. Respiratory control ratio calculated as the ratio of state 3 to state 4° (ADP-stimulated respiration in the presence of pyruvate, malate, and glutamate, following oligomycin treatment). **B.** Coupling control ratio calculated as the ratio of basal or routine respiration (sample in the presence of pyruvate, malate, and glutamate) to state 3, as defined in A. **C.** Flux control ratio for NADH-linked or complex I supported respiration relative to maximal electron transport chain capacity, calculated as the ratio of state 3 to the uncoupled state (FCCP). **D.** Respiratory capacity committed to oxidative phosphorylation (OXPHOS), calculated as the difference in oxygen consumption or flux (JO_2) in the presence of pyruvate, malate, and glutamate following oligomycin treatment. **E.** Respiratory capacity committed to leak respiration, calculated as the difference in JO_2 in the presence of oligomycin following antimycin A treatment. **F.** Maximal respiratory capacity of the electron transport system (ETS), determined as the max JO_2 following FCCP titration. Data are the mean ± S.E.M. for $n = 9-11$ mice per group. The effect of genotype was compared by Student's t-test, where $^*P < 0.05$ and $^{**}P < 0.01$.

function in general [29], or reduced respiratory capacity only in response to stress, but not in healthy mice [15]. Differences between our results and those reported in whole-body *Prkn* knockout mice with regards to hepatic mitochondrial function may reflect systemic metabolic effects of *Prkn* deletion in the whole-body knockout, specifically negative energy balance that impinges upon the liver [29—31] or potentially compensatory changes that occur following germline versus conditional deletion of *Prkn*.

Indeed, the notion that germline deletion of *Prkn* in mice results in compensatory mechanisms to maintain mitochondrial quality control and buffer the cellular response to stress is supported by previous work. Increased rates of autophagy appear to be a compensatory mechanism in skeletal muscle and heart, where increased expression of autophagy genes *Map1lc3* and *Gabarapl1*, and rates of autophagy were reported in whole-body *Prkn* knockout mice [27,49]. Upregulation of PARKIN-independent mitophagy may also buffer the germline loss of *Prkn* in mouse models, as increased *Bnip3* expression is reported in both heart and muscle [27,49], and BNIP3 and LC3 protein levels are increased in mitochondrial fractions from the hearts of *Prkn* knockout mice [27]. Acetaminophen-induced liver injury induces PARKIN-mediated mitophagy; however, *Prkn* knockout mice are protected against acetaminophen toxicity in the liver, in part due to increased rates of hepatocellular proliferation [16]. In contrast, and most relevant to our studies, acute knockdown of hepatic *Prkn* in mice to circumvent compensation using adenoviral-shRNA prevented acetaminophen-induced mitophagy and worsened liver injury [16]. Based on these observations from the literature, it is tempting to speculate that potential compensatory mechanisms were limited in our conditional *Prkn* knockout model and that the observed phenotype is the result of reduced hepatic mitophagy in LKO mice. However, measuring rates of hepatic mitophagy in LKO mice was beyond the scope of our studies and thus limits our interpretation of the potential mechanism by which liver-specific deletion of *Prkn* impairs mitochondrial respiratory function. Studies to determine whether our observed phenotype reflects changes in PARKIN-mediated mitophagy or an alternative function of PARKIN are ongoing and will be of great interest.

Despite these interpretative limitations, recent studies in humans and rodent models suggest that loss of hepatic mitophagy may contribute to the pathogenesis of NAFLD and mark the transition from fatty liver to NASH, consistent with observations made during our studies [11,17]. Hepatic mitophagy flux measured in the mitophagy reporter mouse, mt-Keima, was reduced in obese mice with fatty liver, demonstrating that loss of hepatic mitophagy is associated with NAFLD [17]. Liver biopsy studies in patients representing the breadth of the NAFLD disease spectrum found that increases in mitochondrial respiratory capacity observed in obese subjects were lost in obese patients with NASH, despite the fact that their mitochondrial mass appeared elevated [11]. This very specific observation in patients with NASH, namely mitochondrial dysfunction despite increased mitochondrial mass, is suggestive of reduced mitophagy. Here, by genetically inhibiting PARKIN-mediated mitophagy in the liver through deletion of *Prkn,* we were able to build upon these associative studies and show that in the absence of hepatic PARKIN, the progression of NAFLD was hastened during HFD feeding.

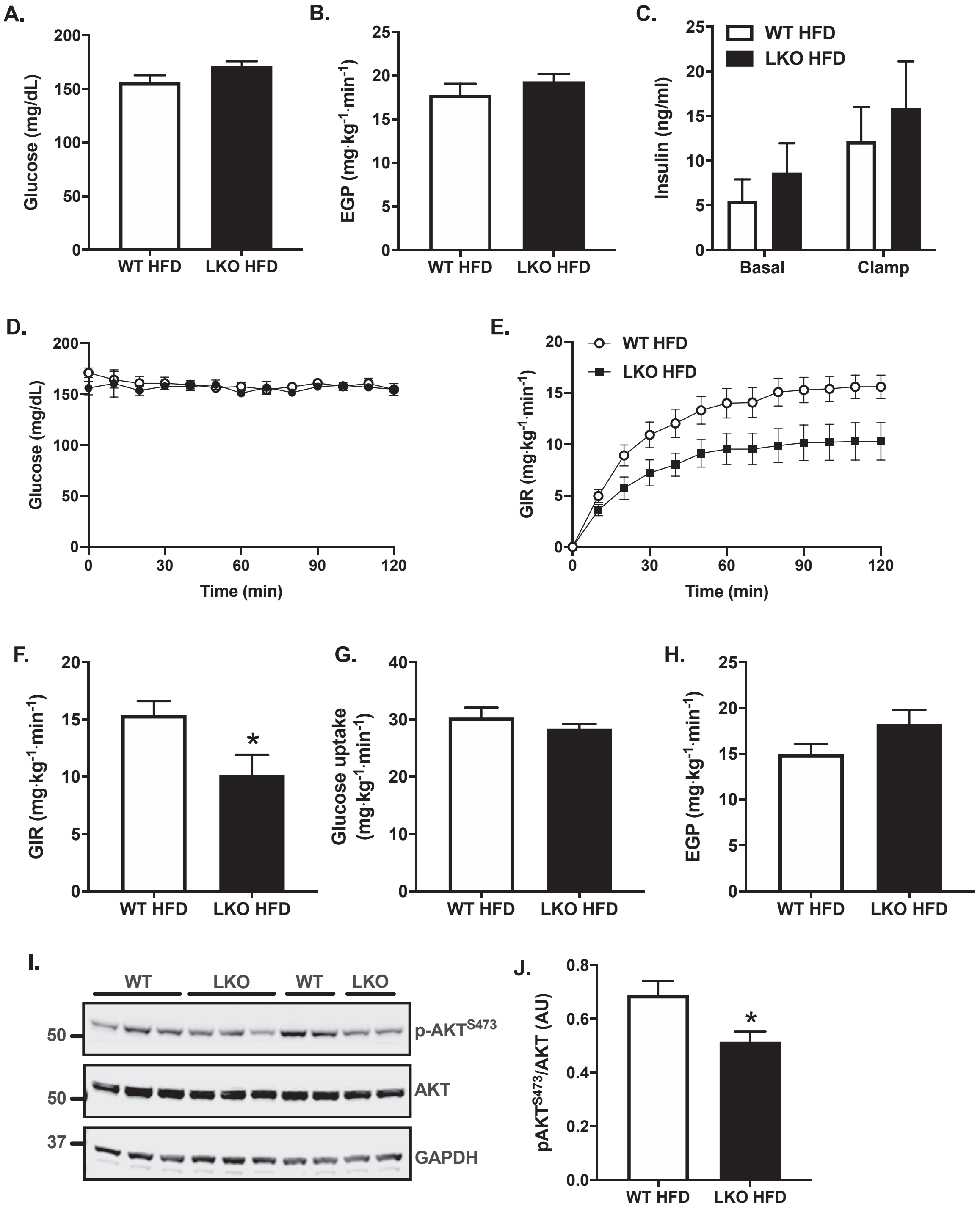

Figure 6: Insulin sensitivity is impaired in liver-specific *Prkn* knockout mice. A. Fasting plasma glucose levels following a six-hour morning fast. **B.** Fasting or basal rates of endogenous or hepatic glucose production (EGP). **C.** Fasting or basal and clamped levels of plasma insulin. **D.** Plasma glucose levels during the hyperinsulinemic infusion. **E.** Glucose infusion rate (GIR) required to maintain euglycemia during the hyperinsulinemic infusion. **F.** The average GIR during the last 40 min or steady-state portion of the clamp. **G.** Whole-body glucose uptake during the clamp. **H.** Insulin-stimulated or clamped rates of EGP. **I.** Western blots of post-clamp liver for indicated target proteins. **J.** Quantification of data in I where AU = arbitrary units. Data are the mean ± S.E.M. for n = 6 mice per group. The effect of genotype was compared by Student's t-test, where $^{*}P < 0.05$.

In summary, we report that liver-specific deletion of PARKIN impairs mitochondrial respiratory capacity and leads to increased hepatic steatosis, insulin resistance, and markers of NAFLD after HFD feeding. These observations, alongside published work describing loss of hepatic mitophagy as an associative feature of NAFLD, suggests that PARKIN-mediated mitophagy maintains mitochondrial integrity *in vivo* and normally protects against diet-induced liver metabolic disease. Together, these studies suggest that strategies to reduce substrate oversupply to the liver or improve mitochondria quality control to avoid or mitigate metabolic stress, respectively, may prevent or slow the pathogenesis of NAFLD.

AUTHOR CONTRIBUTIONS

L.R.E., B.X., A.M.M., B.R.H., J.M., R.U., I.S., A.M., M.P., and M.J.J. performed experiments. M.J.J. conceived the study and designed experiments. L.R.E., A.M., M.P., B.A.K., and M.J.J. analyzed data. B.A.K. and I.S. provided critical input and expertise. L.R.E. and M.J.J. produced figures. L.R.E., I.S., and M.J.J. wrote the manuscript.

ACKNOWLEDGEMENTS

This work was supported by funding from the NIH (R01 DK114012 to M.J.J., T32 DK007052 to A.M.), the American Diabetes Association (1-19-PDF-102 to L.R.E.), the Pittsburgh Foundation (MR2020 109502), and the Pittsburgh Liver Research Center (P30DK120531). The authors thank Drs. Jorge Henao-Mejia and Richard Flavell for help generating the *Prkn* floxed founder mice.

CONFLICT OF INTEREST

None declared.

APPENDIX A. SUPPLEMENTARY DATA

Supplementary data to this article can be found online at https://doi.org/10.1016/j.molmet.2020.101051.

REFERENCES

[1] Data & Statistics and Diabetes | CDC, 2020. National diabetes statistics report. https://www.cdc.gov/diabetes/data/statistics/statistics-report.html. (Accessed 29 April 2020).

[2] Le, M.H., Devaki, P., Ha, N.B., Jun, D.W., Te, H.S., Cheung, R.C., et al., 2017. Prevalence of non-alcoholic fatty liver disease and risk factors for advanced fibrosis and mortality in the United States. PloS One 12(3). https://doi.org/10.1371/journal.pone.0173499.

[3] Williams, C.D., Stengel, J., Asike, M.I., Torres, D.M., Shaw, J., Contreras, M., et al., 2011. Prevalence of nonalcoholic fatty liver disease and nonalcoholic steatohepatitis among a largely middle-aged population utilizing ultrasound and liver biopsy: a prospective study. Gastroenterology 140(1):124—131. https://doi.org/10.1053/j.gastro.2010.09.038.

[4] Loomba, R., Abraham, M., Unalp, A., Wilson, L., Lavine, J., Doo, E., et al., 2012. Association between diabetes, family history of diabetes, and risk of nonalcoholic steatohepatitis and fibrosis. Hepatology (Baltimore, Md.) 56(3): 943—951. https://doi.org/10.1002/hep.25772.

[5] Tilg, H., Moschen, A.R., Roden, M., 2017. NAFLD and diabetes mellitus. Nature Reviews Gastroenterology & Hepatology 14(1):32—42. https://doi.org/10.1038/nrgastro.2016.147.

[6] Begriche, K., Massart, J., Robin, M.-A., Bonnet, F., Fromenty, B., 2013. Mitochondrial adaptations and dysfunctions in nonalcoholic fatty liver disease. Hepatology 58(4):1497—1507. https://doi.org/10.1002/hep.26226.

[7] Sanyal, A.J., Campbell-Sargent, C., Mirshahi, F., Rizzo, W.B., Contos, M.J., Sterling, R.K., et al., 2001. Nonalcoholic steatohepatitis: association of insulin resistance and mitochondrial abnormalities. Gastroenterology 120(5):1183—1192. https://doi.org/10.1053/gast.2001.23256.

[8] Caldwell, S.H., Swerdlow, R.H., Khan, E.M., Iezzoni, J.C., Hespenheide, E.E., Parks, J.K., et al., 1999. Mitochondrial abnormalities in non-alcoholic steatohepatitis. Journal of Hepatology 31(3):430—434.

[9] Cortez-Pinto, H., Chatham, J., Chacko, V.P., Arnold, C., Rashid, A., Diehl, A.M., 1999. Alterations in liver ATP homeostasis in human nonalcoholic steatohepatitis: a pilot study. Journal of the American Medical Association 282(17): 1659—1664.

[10] Szendroedi, J., Chmelik, M., Schmid, A.I., Nowotny, P., Brehm, A., Krssak, M., et al., 2009. Abnormal hepatic energy homeostasis in type 2 diabetes. Hepatology (Baltimore, Md.) 50(4):1079—1086. https://doi.org/10.1002/hep.23093.

[11] Koliaki, C., Szendroedi, J., Kaul, K., Jelenik, T., Nowotny, P., Jankowiak, F., et al., 2015. Adaptation of hepatic mitochondrial function in humans with non-alcoholic fatty liver is lost in steatohepatitis. Cell Metabolism 21(5):739—746. https://doi.org/10.1016/j.cmet.2015.04.004.

[12] Drew, B.G., Ribas, V., Le, J.A., Henstridge, D.C., Phun, J., Zhou, Z., et al., 2014. HSP72 is a mitochondrial stress sensor critical for parkin action, oxidative metabolism, and insulin sensitivity in skeletal muscle. Diabetes 63(5):1488—1505. https://doi.org/10.2337/db13-0665.

[13] Greene, J.C., Whitworth, A.J., Kuo, I., Andrews, L.A., Feany, M.B., Pallanck, L.J., 2003. Mitochondrial pathology and apoptotic muscle degeneration in Drosophila parkin mutants. Proceedings of the National Academy of Sciences of the United States of America 100(7):4078—4083. https://doi.org/10.1073/pnas.0737556100.

[14] Palacino, J.J., Sagi, D., Goldberg, M.S., Krauss, S., Motz, C., Wacker, M., et al., 2004. Mitochondrial dysfunction and oxidative damage in parkin-deficient mice. Journal of Biological Chemistry 279(18):18614—18622. https://doi.org/10.1074/jbc.M401135200.

[15] Williams, J.A., Ni, H.-M., Ding, Y., Ding, W.-X., 2015. Parkin regulates mitophagy and mitochondrial function to protect against alcohol-induced liver injury and steatosis in mice. American Journal of Physiology - Gastrointestinal and Liver Physiology 309(5):G324—G340. https://doi.org/10.1152/ajpgi.00108.2015.

[16] Williams, J.A., Ni, H.-M., Haynes, A., Manley, S., Li, Y., Jaeschke, H., et al., 2015. Chronic deletion and acute knockdown of parkin have differential responses to acetaminophen-induced mitophagy and liver injury in mice. Journal of Biological Chemistry 290(17):10934—10946. https://doi.org/10.1074/jbc.M114.602284.

[17] Sun, N., Yun, J., Liu, J., Malide, D., Liu, C., Rovira, I.I., et al., 2015. Measuring in vivo mitophagy. Molecular Cell 60(4):685—696. https://doi.org/10.1016/j.molcel.2015.10.009.

[18] Lemasters, J.J., 2014. Variants of mitochondrial autophagy: types 1 and 2 mitophagy and micromitophagy (Type 3). Redox Biology 2:749—754. https://doi.org/10.1016/j.redox.2014.06.004.

[19] Matsuda, N., Sato, S., Shiba, K., Okatsu, K., Saisho, K., Gautier, C.A., et al., 2010. PINK1 stabilized by mitochondrial depolarization recruits Parkin to damaged mitochondria and activates latent Parkin for mitophagy. The Journal of Cell Biology 189(2):211—221. https://doi.org/10.1083/jcb.200910140.

[20] Narendra, D., Tanaka, A., Suen, D.-F., Youle, R.J., 2008. Parkin is recruited selectively to impaired mitochondria and promotes their autophagy. The Journal of Cell Biology 183(5):795—803. https://doi.org/10.1083/jcb.200809125.

[21] Iguchi, M., Kujuro, Y., Okatsu, K., Koyano, F., Kosako, H., Kimura, M., et al., 2013. Parkin-catalyzed ubiquitin-ester transfer is triggered by PINK1-dependent phosphorylation. Journal of Biological Chemistry 288(30):22019—22032. https://doi.org/10.1074/jbc.M113.467530.

[22] Kazlauskaite, A., Kondapalli, C., Gourlay, R., Campbell, D.G., Ritorto, M.S., Hofmann, K., et al., 2014. Parkin is activated by PINK1-dependent phosphorylation of ubiquitin at Ser65. Biochemical Journal 460(1):127—139. https://doi.org/10.1042/BJ20140334.

[23] Kane, L.A., Lazarou, M., Fogel, A.I., Li, Y., Yamano, K., Sarraf, S.A., et al., 2014. PINK1 phosphorylates ubiquitin to activate Parkin E3 ubiquitin ligase activity. The Journal of Cell Biology 205(2):143—153. https://doi.org/10.1083/jcb.201402104.

[24] Koyano, F., Okatsu, K., Kosako, H., Tamura, Y., Go, E., Kimura, M., et al., 2014. Ubiquitin is phosphorylated by PINK1 to activate parkin. Nature 510(7503):162—166. https://doi.org/10.1038/nature13392.

[25] Lazarou, M., Sliter, D.A., Kane, L.A., Sarraf, S.A., Wang, C., Burman, J.L., et al., 2015. The ubiquitin kinase PINK1 recruits autophagy receptors to induce mitophagy. Nature 524(7565):309—314. https://doi.org/10.1038/nature14893.

[26] Whitworth, A.J., Theodore, D.A., Greene, J.C., Benes, H., Wes, P.D., Pallanck, L.J., 2005. Increased glutathione S-transferase activity rescues dopaminergic neuron loss in a Drosophila model of Parkinson's disease. Proceedings of the National Academy of Sciences of the United States of America 102(22):8024—8029. https://doi.org/10.1073/pnas.0501078102.

[27] Piquereau, J., Godin, R., Deschênes, S., Bessi, V.L., Mofarrahi, M., Hussain, S.N., et al., 2013. Protective role of PARK2/Parkin in sepsis-induced cardiac contractile and mitochondrial dysfunction. Autophagy 9(11):1837—1851. https://doi.org/10.4161/auto.26502.

[28] Sliter, D.A., Martinez, J., Hao, L., Chen, X., Sun, N., Fischer, T.D., et al., 2018. Parkin and PINK1 mitigate STING-induced inflammation. Nature 561(7722):258—262. https://doi.org/10.1038/s41586-018-0448-9.

[29] Kim, K.-Y., Stevens, M.V., Akter, M.H., Rusk, S.E., Huang, R.J., Cohen, A., et al., 2011. Parkin is a lipid-responsive regulator of fat uptake in mice and mutant human cells. Journal of Clinical Investigation 121(9):3701—3712. https://doi.org/10.1172/JCI44736.

[30] Edmunds, L.R., Huckestein, B.R., Kahn, M., Zhang, D., Chu, Y., Zhang, Y., et al., 2019. Hepatic insulin sensitivity is improved in high-fat diet-fed Park2 knockout mice in association with increased hepatic AMPK activation and reduced steatosis. Physiological Reports 7(21):e14281. https://doi.org/10.14814/phy2.14281.

[31] Costa, D.K., Huckestein, B.R., Edmunds, L.R., Petersen, M.C., Nasiri, A., Butrico, G.M., et al., 2016. Reduced intestinal lipid absorption and body weight-independent improvements in insulin sensitivity in high-fat diet-fed Park2 knockout mice. American Journal of Physiology. Endocrinology and Metabolism 311(1):E105—E116. https://doi.org/10.1152/ajpendo.00042.2016.

[32] Kuznetsov, A.V., Strobl, D., Ruttmann, E., Königsrainer, A., Margreiter, R., Gnaiger, E., 2002. Evaluation of mitochondrial respiratory function in small biopsies of liver. Analytical Biochemistry 305(2):186—194. https://doi.org/10.1006/abio.2002.5658.

[33] Pesta, D., Gnaiger, E., 2012. High-resolution respirometry: OXPHOS protocols for human cells and permeabilized fibers from small biopsies of human muscle. Methods in Molecular Biology (Clifton, N.J.) 810:25—58. https://doi.org/10.1007/978-1-61779-382-0_3.

[34] Kleiner, D.E., Brunt, E.M., Van Natta, M., Behling, C., Contos, M.J., Cummings, O.W., et al., 2005. Design and validation of a histological scoring system for nonalcoholic fatty liver disease. Hepatology (Baltimore, Md.) 41(6):1313—1321. https://doi.org/10.1002/hep.20701.

[35] Kolesar, J.E., Wang, C.Y., Taguchi, Y.V., Chou, S.-H., Kaufman, B.A., 2013. Two-dimensional intact mitochondrial DNA agarose electrophoresis reveals the structural complexity of the mammalian mitochondrial genome. Nucleic Acids Research 41(4):e58. https://doi.org/10.1093/nar/gks1324.

[36] Falabella, M., Kolesar, J.E., Wallace, C., de Jesus, D., Sun, L., Taguchi, Y.V., et al., 2019. G-quadruplex dynamics contribute to regulation of mitochondrial gene expression. Scientific Reports 9(1):5605. https://doi.org/10.1038/s41598-019-41464-y.

[37] Livak, K.J., Schmittgen, T.D., 2001. Analysis of relative gene expression data using real-time quantitative PCR and the 2(-Delta Delta C(T)) Method. Methods (San Diego, Calif.) 25(4):402—408. https://doi.org/10.1006/meth.2001.1262.

[38] Millar, J.S., Cromley, D.A., McCoy, M.G., Rader, D.J., Billheimer, J.T., 2005. Determining hepatic triglyceride production in mice: comparison of poloxamer 407 with Triton WR-1339. Journal of Lipid Research 46(9):2023—2028. https://doi.org/10.1194/jlr.D500019-JLR200.

[39] Henao-Mejia, J., Williams, A., Rongvaux, A., Stein, J., Hughes, C., Flavell, R.A., 2016. Generation of genetically modified mice using the CRISPR-cas9 genome-editing system. Cold Spring Harbour Protocols 2016(2):prot090704. https://doi.org/10.1101/pdb.prot090704.

[40] Chaugule, V.K., Burchell, L., Barber, K.R., Sidhu, A., Leslie, S.J., Shaw, G.S., et al., 2011. Autoregulation of Parkin activity through its ubiquitin-like domain. The EMBO Journal 30(14):2853—2867. https://doi.org/10.1038/emboj.2011.204.

[41] Puri, P., Wiest, M.M., Cheung, O., Mirshahi, F., Sargeant, C., Min, H.-K., et al., 2009. The plasma lipidomic signature of nonalcoholic steatohepatitis. Hepatology (Baltimore, Md.) 50(6):1827—1838. https://doi.org/10.1002/hep.23229.

[42] Younossi, Z.M., Loomba, R., Anstee, Q.M., Rinella, M.E., Bugianesi, E., Marchesini, G., et al., 2018. Diagnostic modalities for nonalcoholic fatty liver disease, nonalcoholic steatohepatitis, and associated fibrosis. Hepatology 68(1):349—360. https://doi.org/10.1002/hep.29721.

[43] Brand, M.D., Nicholls, D.G., 2011. Assessing mitochondrial dysfunction in cells. Biochemical Journal 435(2):297—312. https://doi.org/10.1042/BJ20110162.

[44] Samuel, V.T., Petersen, K.F., Shulman, G.I., 2010. Lipid-induced insulin resistance: unravelling the mechanism. Lancet (London, England) 375(9733):2267—2277. https://doi.org/10.1016/S0140-6736(10)60408-4.

[45] Samuel, V.T., Shulman, G.I., 2012. Integrating mechanisms for insulin resistance: common threads and missing links. Cell 148(5):852—871. https://doi.org/10.1016/j.cell.2012.02.017.

[46] Summers, S.A., 2010. Sphingolipids and insulin resistance: the five Ws. Current Opinion in Lipidology 21(2):128—135. https://doi.org/10.1097/MOL.0b013e3283373b66.

[47] Satapati, S., Sunny, N.E., Kucejova, B., Fu, X., He, T.T., Méndez-Lucas, A., et al., 2012. Elevated TCA cycle function in the pathology of diet-induced hepatic insulin resistance and fatty liver. Journal of Lipid Research 53(6):1080—1092. https://doi.org/10.1194/jlr.M023382.

[48] Satapati, S., Kucejova, B., Duarte, J.A.G., Fletcher, J.A., Reynolds, L., Sunny, N.E., et al., 2015. Mitochondrial metabolism mediates oxidative stress and inflammation in fatty liver. Journal of Clinical Investigation 125(12):4447—4462. https://doi.org/10.1172/JCI82204.

[49] Gouspillou, G., Godin, R., Piquereau, J., Picard, M., Mofarrahi, M., Mathew, J., et al., 2018. Protective role of Parkin in skeletal muscle contractile and mitochondrial function. The Journal of Physiology 596(13):2565—2579. https://doi.org/10.1113/JP275604.